Eur. Phys. J. E **8**, 275–282 (2002)
DOI 10.1140/epje/i2001-10101-0

THE EUROPEAN PHYSICAL JOURNAL E
EDP Sciences
© Società Italiana di Fisica
Springer-Verlag 2002

Dewetting of solid-supported multilamellar lipid layers

L. Perino-Gallice[1], G. Fragneto[1], U. Mennicke[2], T. Salditt[2], and F. Rieutord[3,a]

[1] Institut Laue-Langevin, B.P. 156, 38042 Grenoble Cedex 9, France
[2] Universität des Saarlandes, Postfach 15 11 50, 66041 Saarbrücken, Germany
[3] CEA-Grenoble Département de Recherche Fondamentale sur la Matière Condensée, 38054 Grenoble Cedex 9, France

Received 27 November 2001

Abstract. Thin multilamellar assemblies of neutral lipid bilayers deposited on silicon substrates are shown to be unstable upon hydration. We analyze the stability of these systems taking into account a reduction of the fluctuation-related components of the bilayer interaction potential. The sizes of the patterns observed are consistent with a spinodal dewetting process.

PACS. 68.08.Bc Wetting – 87.16.Dg Membranes, bilayers, and vesicles

1 Introduction

For years, amphiphilic lipid layers have attracted the interest of physicists, as model systems for biological membranes. The quantitative understanding of lipid model systems often starts from structural investigations. Cell membranes are mainly formed by lipids and proteins, with the lipids organised in the form of a double sheet (lipid "bilayer"). One of the simplest ways to model membranes is to prepare bilayers made of pure neutral lipids. These lyotropic systems exhibit a wealth of different phases as a function of temperature and hydration, due to the interplay of different forces [1]. However, the exact balance of these interactions is unclear. Phenomena like anomalous swelling at the gel/liquid phase transition of the aliphatic chains [2–5] or the so-called "vapor pressure paradox" [6–8] are still objects of controversy.

Among many different systems used to study membrane physical interactions the most extensively studied models are multilamellar vesicles in aqueous medium [9–11]. Stacks consisting of hundreds of bilayers deposited on solid substrates and hydrated by contact with water vapor [4,12–14] have allowed more detailed structural studies since the broad orientation distribution that is present in multilamellar vesicles is suppressed [8].

Such thick stacked multibilayers have the drawback that only the properties averaged over hundreds of bilayers can be determined. On the other hand, single adsorbed bilayers interact strongly with the substrate. For detailed investigation, a compromise could be the formation of only few bilayers that are likely to be more stable in bulk water and are sufficiently thin that the characteristics of each bilayer can be determined separately, *e.g.* their structure with Å resolution, by techniques like specular and off-specular reflectivity. We have recently succeeded in the preparation of samples with a well-controlled number N of bilayers (typically less than ten), spin-coated on silicon wafers [15], and have started their characterisation with X-rays. Here we present results from neutron reflectivity as well as atomic-force microscopy (AFM) and optical microscopy measurements on this new model system of solid-supported membranes.

Neutron reflectivity has been extensively used for the *in situ* characterization of soft-condensed-matter systems at interfaces. It is an attractive technique since it has a resolution of less than a nanometer, it is non-destructive and isotopic substitution can be used for highlighting specific parts of the system. Light elements such as carbon, hydrogen, nitrogen and oxygen are relatively strong scatterers for neutrons which makes them particularly well suited for the study of biological material. Specular neutron reflectivity gives information on the structure perpendicular to the plane of the membranes, while the lateral structure is averaged. In order to obtain complementary information on the lateral structure, observations of the surface of the samples using standard optical microscopy and AFM were performed. The systems were found to be intrinsically unstable and inclined to form inhomogeneous structures reminiscent of what is observed when dewetting occurs in thin films of liquid crystals or polymers. AFM observations, consistent with the reflectivity results, are interpreted in the framework of spinodal dewetting theory. A detailed analysis of the interaction potentials within the multilayer stacks and their evolution upon hydration is given in support to the interpretation. The initial motivation for this work was the study of the interaction of the lipids with the peptide alamethicin [14,16,17]. Indeed, both neutron reflectivity and AFM measurements

[a] e-mail: rieutord@cea.fr

have also been performed on systems including different proportions of alamethicin (ranging from 1/200 to 1/10 peptide/lipid ratios) all showing similar results as those reported here for pure lipids. As the presence of the peptide makes the analysis more complicated, its effect can be quantitatively estimated only after a full understanding of the model system. The results of the effect of the peptide will be the object of a future publication.

2 Materials and methods

Chemicals

1,2-dimyristoyl-sn-glycero-3-phosphatidylcho-line (DMPC) with different isotopic compositions was purchased from Avanti Polar Lipids, Alabama (USA), and used without further purification. Fully-deuterated(d_{67}-DMPC), chain-deuterated (d_{54}-DMPC) and head-deuterated (d_{13}-DMPC) lipids were used. Multilamellar bilayers were prepared on clean silicon substrates by spreading from an organic solution. The lipids were dissolved in isopropanol at a concentration of 5 mg/ml. The 5 cm diameter substrates were cleaned in methanol followed by extensive rinsing in ultrapure water (specific resistivity 18 MΩ cm, Millipore, Bedford, MA). They were made hydrophilic by immersion into a saturated solution of KOH in ethanol for about one minute. Finally, they were rinsed several times in ultra-pure water.

Deposition

The deposition was made at room temperature by spin-coating. In order to obtain samples with less than 10 lipid bilayers, a drop of 500 μl was spread on the substrate surface in rotation at a speed of 1000 rpm. After one second, the speed was increased to 5000 rpm for 30 s. The samples were then put under vacuum for about 8 hours to remove the solvent. Then the samples were kept in air at 8 °C, until the measurement.

Reflectivity measurements and analysis

Specular reflectivity, defined as the ratio between the intensity of the specularly reflected beam, I, and that of the incoming beam, I_0, is measured as a function of the wave vector transfer $q = \frac{4\pi}{\lambda}\sin\theta$, perpendicular to the reflecting surface, where λ is the wavelength of the neutron beam and θ the incident angle. This signal is a function of the scattering length density across the interface, $\rho(z)$. An expression within the Born approximation is given by [18]

$$I/I_0 \approx \frac{16\pi^2}{q_z^2}|\tilde{\rho}(q_z)|^2\,, \qquad (1)$$

where $\tilde{\rho}(q_z)$ is the Fourier transform of $\rho(z)$. Measurements were performed at the Institut Laue Langevin on the D16 diffractometer adapted for reflectivity measurements [19]. A monochromatic neutron beam (wavelength $\lambda = 4.52$ Å with a wavelength spread $\Delta\lambda/\lambda \approx 0.02$) was collimated by two sets of slits located in front of the sample position. Neutrons specularly reflected off the sample were detected using a two-dimensional ^{3}He detector placed at a 1 m distance from the sample. The reflected intensity was measured as a function of the glancing angle of incidence θ by rotating the sample. The detector was kept at 3 different fixed positions covering the angular θ range 0–7.12 °. Samples were hydrated in a temperature-controlled hydration chamber. The chamber (adapted from [20]) consists of two thermally insulated compartments that can be kept at different temperatures by water circulation. In the lower compartment, there is a water reservoir set at a temperature $T_{\rm L}$. In the upper part, equilibrated at temperature $T_{\rm U}$, sits the sample. A small aperture allows the exchange of water vapor between the two chambers. Such a chamber allows one to set an osmotic pressure Π, given by the temperature difference between the lower and the upper chambers: $\Pi = -\frac{k_{\rm B}T_{\rm U}}{V_{\rm w}}\ln(\frac{p_{\rm L}}{p_{\rm U}})$ where $p_{\rm L}$ and $p_{\rm U}$ are the equilibrium pressures of water vapor at $T_{\rm L}$ and $T_{\rm U}$, respectively, $k_{\rm B}$ is the Boltzman constant and $V_{\rm w}$ the molecular volume of water. For this work both chambers were thermalized by the same waterbath, the warm water entering the lower part first so that $T_{\rm U} \lesssim T_{\rm L}$. As the sample temperature can only be lower than $T_{\rm U}$ (no external heat supply), we expect the sample to be the coolest point of the system and hence to be facing a vapor phase of 100 per cent relative humidity (no osmotic stress). Measurements were performed at about 45 °C, a temperature where DMPC is in the fluid phase L_α. The samples were kept at this temperature for one hour before starting the measurement, as had been verified that the reflectivity profile did not show changes after this time and it was assumed that the system had equilibrated.

Optical and atomic force microscopies

Optical microscopy and AFM were used to observe the in-plane structure of the samples before and after hydration [21]. All experiments were carried out at room temperature. AFM measurements were performed using a Park Scientific Instrument Autoprobe CP microscope operating in the tapping mode. All images have been obtained using soft cantilevers (bending rigidity 0.3 N/m, resonance frequency of 18 kHz) and a scanning frequency of 1 Hz/line. Samples were hydrated using the same temperature-controlled hydration chamber as the one used for the neutron reflectivity measurements. Samples were observed in air at room temperature immediately after hydration.

3 Results and discussion

Reflectivity measurements and analysis

Neutron reflectivity profiles were measured on DMPC and d_{67}-DMPC samples in D_2O, and d_{54}-DMPC, d_{13}-DMPC

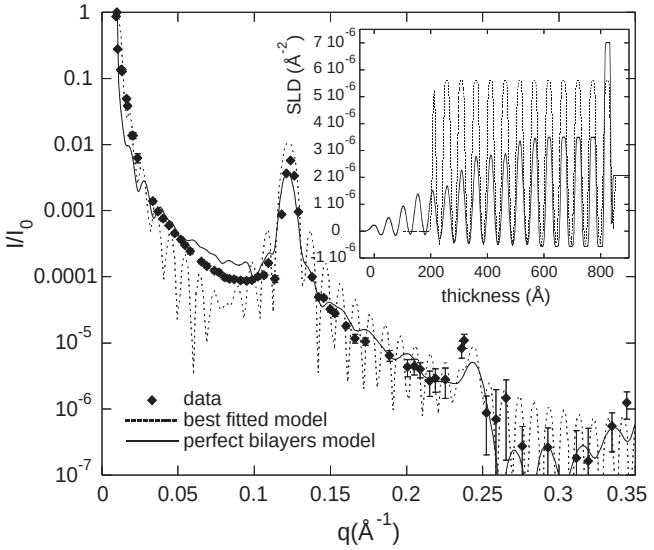

Fig. 1. (•) Reflectivity data from d_{54}-DMPC sample in 100% r.h. H_2O vapor. Dashed line: simulation obtained from theoretical SLD values ($SLD_{tails} = 7.13 \cdot 10^{-6}$ Å^{-2} and $SLD_{heads} = 1.75 \cdot 10^{-6}$ Å^{-2}). Solid line: best fit to the data. Insert: corresponding scattering length density (SLD) profiles.

and d_{67}-DMPC samples in H_2O. Data were analysed by model fitting with a standard Parratt [22] algorithm using the exact optical matrix formulation of reflectivity [23]. The first step was to compare the data with a model of the system consisting of homogeneous bilayers, well aligned with respect to the substrate and separated by a water film. The scattering length densities for the DMPC molecules were fitted around their literature values. These were obtained from atomic scattering length densities [24] and molecular volumes taken in reference [25]. The thickness and roughness parameters were fitted starting from the parameters obtained from previous measurements [19]. For all measured samples, the total repeat distance, deduced from the Bragg peak positions ($q_{001} \approx 0.12$ Å^{-1} and $q_{002} \approx 0.24$ Å^{-1}), was found to be $d = 52 \pm 1$ Å and the bilayer thickness was $d_B = 39 \pm 1$ Å (see Fig. 5 below) with a head-group thickness of 7.5 ± 1 Å and a tail thickness of 12.0 ± 1 Å. The r.m.s. roughness was about $\sigma = 4$ Å. The number N of periods in the system, obtained from the width of the Bragg peaks, was found to correspond to about $N = 10$ bilayers. For example, Figure 1 shows the experimental data obtained for d_{54}-DMPC in H_2O vapor humidity along with a simulated reflectivity profile obtained from a homogeneous-layer hypothesis (Fig. 1 (dashed line)). The corresponding scattering length density profile is given in the insert. Similar results were obtained for all the measured reflectivity profiles. As the layers were supposed to be perfect and well aligned, the simulation exhibits well-defined Kiessig fringes. Such fringes are due to the interference between the external interfaces of the system. They are not observed on the experimental curve. This can be already interpreted by a large degree of disorder at the surface of the sample. Note that if the disorder had affected the multilamellar stacking, the Bragg peaks would have disappeared as well and in particular at high wave vectors. However, the presence of the third order ($q = 0.35$ Å^{-1}) indicates that the internal structure at small scale is still well defined. A better fit to the data was obtained only when the scattering length density (SLD) and roughness of the lipid layers were allowed to change across the sample (see Fig. 1 (solid line)). The scattering length density profile obtained (see insert, solid line) shows that it decreases with the distance from the substrate. In the present example, this can be interpreted with a decreasing amount of matter in each layer. The first bilayer, highly anchored on the substrate, keeps an SLD close to the theoretical one, while that of the last bilayer decreases to about 10% of the theoretical one. The total number of layers had to be increased, with respect to the model found with the theoretical values of SLD, in order to compensate for the reduced contrast of individual layers affecting the Bragg peaks intensity.

This result is surprising and it seems general to all multilamellar systems we have looked at. To our knowledge, it has never been observed before. A reason may be that most experiments reported in the literature were carried out on samples formed by a large number of bilayers (typically several hundreds). Because of the large number of bilayers, the Kiessig fringes spacing on such systems is too small compared to the instrumental resolution and fully compact system models were used to describe the data [14].

Optical microscopy and AFM observations

Figure 2(a) shows an AFM image of a partially deuterated (d_{54}-DMPC) sample stored in air for one week after fabrication. The AFM measurement was done at room temperature and before hydration. Most of the surface is flat and no detectable features were observed by optical microscopy. However, a few holes with diameters ranging from 2 to 6 μm and depths ranging from 130 to 330 Å are observed by AFM. All the patterns observed show a minimum thickness variation unit. This unit thickness variation corresponds to the multilamellar repeat distance of about 52 Å . After 4 hours of hydration at a temperature of 45 °C, a dramatic change in the surface morphology is observed (see the AFM image in Fig. 2(b) and optical-microscopy image in Fig. 3). The hydration has triggered a large reorganisation at the surface which presents an array of large holes and patches. The maximum thickness between the holes and the top of the patches is of about 1200 Å. The AFM observations indicate, in agreement with the reflectivity measurements, that the multilamellar nature of the stack is preserved (also shown in Fig. 4). The empty zones (clear areas in Fig. 3) are not totally free of material as a few shallow holes can still be observed using AFM in these areas (see Fig. 2(b)). This observation is consistent with the reflectivity measurement analysis which suggests the existence of a lipid bilayer strongly adsorbed on the substrate. It is also consistent with our experience from Langmuir-Blodgett transfer of DMPC layers: while it is relatively easy to transfer two lipid monolayers

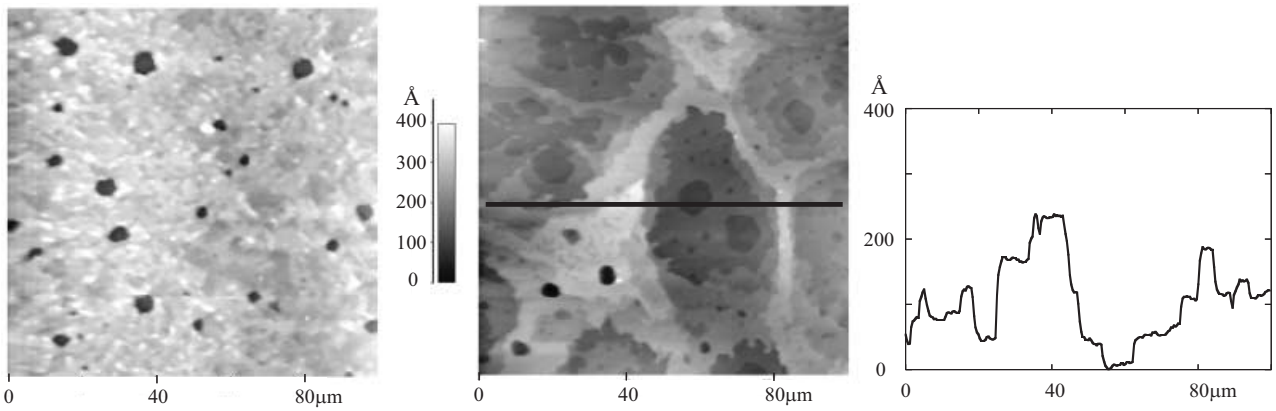

(a) (b) (c)

Fig. 2. AFM images of multilamellar lipid layers sample before hydration (a) and after hydration (dewetted sample) at 45 °C (b), cross-section along the black line (c).

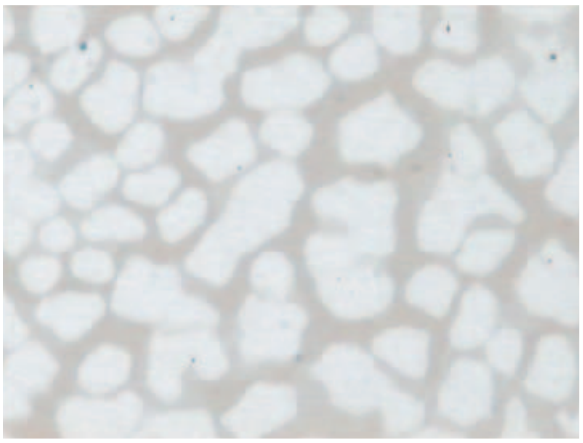

Fig. 3. View by optical microscopy (thicker stacks in grey) of a DMPC sample surface after hydration at 45 °C during 4 h. The full width of the image is 100 μm.

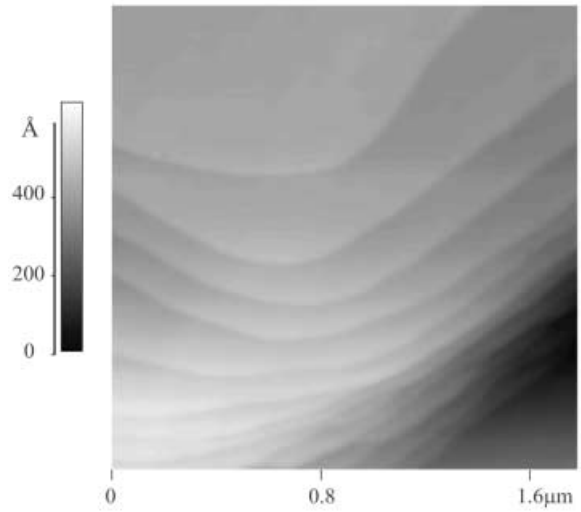

Fig. 4. View by AFM of the extremity of a patch of a hydrated DMPC sample. The step height corresponds to one bilayer.

(one bilayer) by this method, the transfer rate drops considerably when one attempts to build up more layers. The interactions between a hydrophilic substrate and a bilayer are strong but the interaction between DMPC bilayers is too weak to allow the deposition of other bilayers.

Interpretation of the structure

The patterns observed after hydration are highly similar to the dewetted surface of a liquid crystal film as observed, *e.g.*, by Herminghaus *et al.* (see [26], Fig. 2(a)). The structure was explained, in that case, by spinodal dewetting, *i.e.* by an instability induced by the development of a surface fluctuation. Fluctuations and undulations are known to play a large role in the interactions between the layers in multilamellar systems and we examine here what conclusions can be drawn by using this framework.

For an instability to be present in a thin film, the interaction force between the liquid/vapor and solid/liquid interface (*i.e.* the so-called "disjoining pressure") has to become less attractive when the thickness increases and more attractive when it decreases. Then an excitation at the surface may destabilize the film [27]. The predictions of such a model are described below. If the excitation is written as

$$h(x,t) = h_0 + \xi_0 e^{-t/\tau} \sin(qx)\,, \qquad (2)$$

where h is the film thickness at the position x in the plane of the interface at time t, h_0 the initial thickness, ξ_0 the initial amplitude of the fluctuation supposed to be small ($\xi_0 \ll h_0$), τ the characteristic time and q the wave vector, then the dewetting conditions can be expressed in terms of the effective potential of the film interfaces interactions $\phi(h)$, *i.e.* the free energy of the film per unit surface [28].

By writing down a linearized version of the fluid motion induced in the film under the action of Laplace and disjoining pressures (the deformation of the surface due to

the fluctuation induces a Poiseuille flow in the film), one can work out an expression for the time evolution of the perturbation as a function of the wave vector [27,29,30]:

$$\frac{1}{\tau} = \frac{h_0^3}{3\eta} q^2 \left(\gamma q^2 + \frac{\partial^2 \phi(h)}{\partial h^2} \right), \tag{3}$$

where γ is the surface tension and η the viscosity of the film. A perturbation will increase if $\frac{1}{\tau} < 0$. As a consequence, the film is always stable for $\partial^2\phi(h)/\partial h^2 > 0$. When $\partial^2\phi(h)/\partial h^2 < 0$, the surface will be unstable against perturbations of wave vectors lower than the critical wave vector $q_\mathrm{c} = \sqrt{\frac{-\partial^2\phi(h)/\partial h^2}{\gamma}}$. In this spinodal dewetting model, it is assumed that the observed final patterns correspond to the fastest growing mode, which has a wave vector q_M,

$$q_M = \sqrt{\frac{-\partial^2\phi(h)/\partial h^2}{2\gamma}}. \tag{4}$$

The characteristic time for the instability to develop is given by τ_M:

$$\frac{1}{\tau_M} = \frac{h_0^3}{12\gamma\eta} \cdot \left| \frac{\partial^2\phi(h)}{\partial h^2} \right|^2, \tag{5}$$

as obtained from a linear perturbation theory. It should be noted that both equations (4) and (5) do not include dependence on the relative values of surface tensions ($\gamma_\mathrm{sf} + \gamma_\mathrm{fv}$) and γ_sv, where γ_sf, γ_fv and γ_sv are the solid/film, film/vapor and solid/vapor surface tensions, respectively. These quantities play a role only when late stages of dewetting are considered, if "dry" surface areas appear on the substrate.

Models for the potential

The previous expression shows that the behaviour is determined by the interaction potential describing the way the system will react to a perturbation. We shall here address the question of establishing an expression for the potential $\phi(h)$. Let us first consider the system as homogeneous with van der Waals interactions only. Then [31]

$$\phi(h) = \gamma_\mathrm{sl} + \gamma_\mathrm{lv} - \frac{A}{12\pi h^2}. \tag{6}$$

The last term corresponds to the van der Waals potential interaction between the solid/liquid and liquid/air interface. A is the Hamaker constant for the air/film/substrate system. Note that we use here the sign convention of reference [31], where $A > 0$ means attractive forces between the interfaces (opposite to that of Ref. [27]). In this assumption,

$$\frac{\partial^2\phi}{\partial h^2} = -\frac{A}{2\pi h^4}. \tag{7}$$

Then the instability develops if $A > 0$. Typically, A can be estimated *via* a calculation within the full Lifshitz theory [31]. The film material is considered as having a dielectric constant and refractive index obtained from those of an aliphatic medium and water at a ratio of $52/(52-39)$. The parameters used are shown in footnote [1], the absorption frequency of all media has been taken equal to 3×10^{15} s^{-1} [31]. The calculation gives $A \approx -1.6 \cdot 10^{-19}$, *i.e.* it predicts a complete wetting of the lipidic film on the substrate and the stability of this film, contrary to the observations. The discrepancy between the predictions of the pure van der Waals model and the experimental observations in hydrocarbon/water systems is fairly common and calls for the consideration of other forces [31] or, in this case, the consideration of the nanoscale structure of the film. Here, the system is composed of a stack of bilayers and we can assume that it will react to a perturbation applied to its surface as a sum of the individual contributions of each bilayer composing the stack. The swelling of a multilamellar stack and especially the equilibrium distance obtained is due to a balance between the different interactions in the system which include attractive van der Waals forces, f_vdW, repulsive interactions due to fluctuations, f_fl [32], and hydration forces f_hyd, so that the resulting force f acting on a bilayer can be written as

$$f(z,\delta) = f_\mathrm{vdW}(z,\delta) + f_\mathrm{fl}(z,\delta) + f_\mathrm{hyd}(z,\delta); \tag{8}$$

z is the repeat period of the membranes, δ the thickness of the dry lipid, ($z-\delta$ is the water interlayer thickness). The first term is the bilayer/bilayer van der Waals interaction potential given by

$$\Phi_\mathrm{vdW}(z,\delta) = -\frac{A}{12\pi}\left[\frac{1}{(z-\delta)^2} - \frac{2}{(z)^2} + \frac{1}{(z+\delta)^2}\right]. \tag{9}$$

The second and third terms represent the repulsive potential due to fluctuations (entropic confinement) and hydration. Here we used expressions of the form [33,34]

$$\Phi_\mathrm{fl}(z,\delta) = \frac{\pi k_\mathrm{B} T}{16}\left(\frac{A_H}{\kappa\lambda_\mathrm{fl}^2}\right)^{1/2} \exp\left(-\frac{(z-\delta)}{\lambda_\mathrm{fl}}\right) \tag{10}$$

and

$$\Phi_\mathrm{hyd}(z,\delta) = A_H \exp\left(-\frac{(z-\delta)}{\lambda_\mathrm{hyd}}\right). \tag{11}$$

κ is the bending rigidity of the bilayer, λ_fl the decay length and A_H a prefactor related to the compressibility of the bilayer. The decay length λ_hyd is approximatively half of the decay length of the repulsive force due to fluctuations λ_fl and it is typically of the order of a water molecule size. This form was shown to account well for osmotic stress experiments data [12,35].

Note that the separation in the physical origins of the two repulsive terms above is somewhat arbitrary, though.

[1]

	Silicon	DMPC+H_2O	Air
ϵ	12	25	1
n	3,5	1,45	1

Dielectric constant at zero frequency and optical index of the different media. The index of the film has been calculated with those of lipids and water [31].

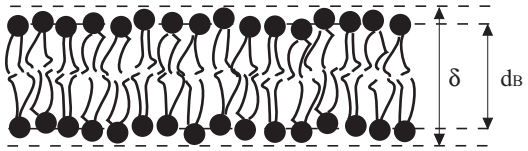

Fig. 5. Definition of the bilayer thickness parameters (see text for details).

The hydration term is enhanced by fluctuations because two fluctuating membranes can come locally very close to each other and experience this repulsion. Symmetrically, the entropic confinement term will be dependent on the range of the hydration interaction potential between membranes [36].

The decay of all interactions is fast enough to consider only the interactions between neighboring membranes. If N is the number of bilayers in the stack, the total interaction potential can be written as

$$\phi_{\rm tot}(h) = N\Phi(z,\delta)\,. \tag{12}$$

$\phi_{\rm tot}$ is then equal to N times a function of the swelling factor $g = z/\delta$ as variable. The effective potential Φ per bilayer can be written in terms of this variable:

$$\begin{aligned}\Phi(g) = {} & \frac{\pi k_{\rm B}T}{16}\left(\frac{A_H}{\kappa\lambda^2}\right)^{1/2}\exp\left(-\frac{(g-1)}{2\lambda/\delta}\right) \\ & + A_H\exp\left(-\frac{(g-1)}{\lambda/\delta}\right) \\ & - \frac{A}{12\pi\delta^2}\left[\frac{1}{(g-1)^2} - \frac{2}{g^2} + \frac{1}{(g+1)^2}\right],\end{aligned} \tag{13}$$

where $\lambda = \lambda_{\rm hyd}$.

In agreement with previous work, the lipid/water/lipid Hamaker constant has been taken equal to 0.7×10^{-20} J [31]. It is positive and the van der Waals forces between lipid bilayers are attractive. We used the values $A_H = 0.035$ J/m^2, $\lambda = 1.94$ Å and $\kappa = 0.55 \times 10^{-19}$ J in equation (13) which were shown to account well for the osmotic stress experimental measurements on this system [12]. It should be noted that, in this study, the parameter δ corresponding to the bilayer thickness is not the same as the parameter $d_{\rm B}$ determined from reflectivity measurements, as it includes the fluctuations amplitude (see Fig. 5). In such a description, the bilayer thickness must be increased by 5 Å [37] so that $\delta = 44 \pm 1$ Å. With these parameters, expression (13) predicts a stable minimum for a swelling factor of $g = 1.46$. Experimentally for a fully hydrated system of DMPC, the repeat distance is 64 Å corresponding to $g = 1.42$.

Let us now consider a system made of a few periods where interfaces are expected to reduce strongly the fluctuations. This system exhibits a repeat distance of 52 Å corresponding to a swelling factor $g = 1.15$. The fact that we do not obtain the same swelling factor for our system as the one of fully hydrated bilayers immersed in water can be considered as another manifestation of the so-called "vapor pressure paradox". The same reduced value for the swelling factor has been observed already by several teams who were not able to find, in water-saturated vapor, a hydration level comparable to that found for lipid bilayers immersed in bulk water, although the two experimental conditions correspond to the same chemical potential. Two explanations have been put forward to explain this paradox:

- (a) A theoretical one was suggested by Podgornik *et al.* [6]. The stack of bilayers exposed to a saturated water vapor is bound by surfaces under tension. This tension leads to an important decrease of the fluctuations of the external layers. The perturbation of the fluctuations by surface tension terms has a large decay length and extends to the entire system. It is well known that for such lipid systems, an important part of the swelling is due to repulsion stemming from fluctuations. The reduced fluctuations result then in a decrease of the hydration level. Experiments by Tristram-Nagle *et al.* were interpreted as supporting this theory [7].
- (b) A technical one, given by Katsaras [38], who suggested that there are always small temperature gradients in a hydration vessel so that the relative humidity is never 100%. As a demonstration, the authors showed that it was possible to hydrate *via* vapor, using a carefully designed set-up, thick stacks of bilayers to the same swelling factor as lipid bilayers immersed in bulk water. These results, however, do not contradict interpretation (a) as it was proposed [8] that, in such case, the presence of additional water layer at the boundaries of the multilamellar stack makes it loosely coupled to its interfaces.

Here we consider a system formed by less than ten membranes so that the effects of the air/lipid and lipid/solid interfaces and the corresponding surface tension should be particularly important. We now address the question of how the reduction of fluctuations could affect the interaction potential $\Phi(z)$. The main consequence in terms of free energy of the system is that the repulsive terms of equation (13) are reduced when fluctuations are suppressed.

To parametrize this reduction, we have applied a common reduction factor r to the repulsive part of the potential as a simple way to account for the interplay between direct and entropic interactions. Indeed, previous studies have shown that a strong renormalization of the direct interactions by the fluctuations takes place in these systems [39]. The potential now reads

$$\Phi_r(g) = \frac{1}{r}\left[\Phi_{\rm fl} + \Phi_{\rm hyd}\right] + \Phi_{\rm vdW}. \tag{14}$$

The parameter r quantifies the inhibition of undulation interaction by interfaces. Its absolute value does not have any direct meaning and it should be only considered as a crude approximation to more sophisticated approaches which would have to be used in a next step by explicitly taking into account the effect of surface tension on the fluctuation amplitude [6,40,41]. Within this assumption,

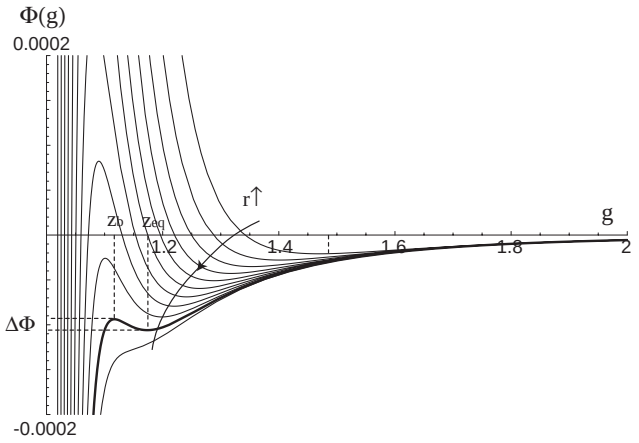

Fig. 6. Evolution of the interaction potential Φ as a function of the swelling factor g for different values of the fluctuation reduction factor r. r ranges from 1 to 6 by steps of 0.5.

the effective potential can be written as

$$\Phi_r(g) = \frac{1}{r}\left[\frac{\pi k_{\mathrm{B}}T}{16}\left(\frac{A_H}{\kappa\lambda^2}\right)^{1/2}\exp\left(-\frac{(g-1)}{2\lambda/\delta}\right) + A_H\exp\left(-\frac{(g-1)}{\lambda/\delta}\right)\right] - \frac{A}{12\pi\delta^2}\left[\frac{1}{(g-1)^2} - \frac{2}{g^2} + \frac{1}{(g+1)^2}\right]. \quad (15)$$

Figure 6 presents the modified potential $\Phi_r(g)$ as a function of the swelling rate g for different values of r. When r is increased, the minimum is shifted from $g = 1.46$ (value obtained with the total potential, $r = 1$) to smaller values as the attractive part due to van der Waals takes over the weakened repulsive fluctuation part. As long as r is small enough ($r < 5.8$), the interaction potential keeps a minimum at the position g_0, where the system is in equilibrium. Moreover, this equilibrium situation is stable as $\Phi_r''(g_0) > 0$.

Figure 7 shows the stability domain in a two-dimensional space: swelling factor (g) *vs.* repulsive damping factor (r). The dashed line represents the position of the equilibrium swelling factor as a function of r, *i.e.* the position of the minimum of potential when no external pressure is applied. The large dot is the equilibrium position for lipid bilayers in bulk water. If $r > 5.8$ the equilibrium line crosses the stability domain boundary: attractive interactions are now dominant and the system becomes unstable. It is a remarkable prediction of this simple model that the swelling factor, $g = 1.14$, at which this occurs is very close to the swelling factor observed on our system ($g = 1.15$). The hydration level which is obtained in experiments corresponds to the stability limit of the system. Upon further reduction of the repulsive terms, the system would become mechanically unstable and evolve discontinuously to another minimum.

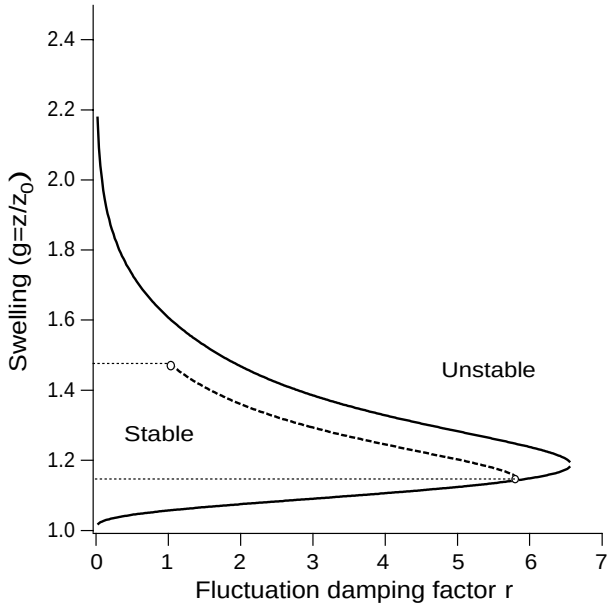

Fig. 7. Stability domain as a function of g and r. Dashed line: equilibrium position location.

Prediction of the dewetting pattern wavelength

Thermal fluctuations can induce dewetting as soon as the energy barrier which the system has to overcome to escape from its local minimum is of the order of $k_{\mathrm{B}}T$:

$$\Delta\phi_{\mathrm{tot}} = \phi_{\mathrm{tot}}(h_{\mathrm{b}}) - \phi_{\mathrm{tot}}(h_{\mathrm{eq}}) \approx k_{\mathrm{B}}T\,,$$

where $h_{\mathrm{b}} = nz_{\mathrm{b}} = ng_{\mathrm{b}}\delta$ and $h_{\mathrm{eq}} = nz_{\mathrm{eq}} = ng_{\mathrm{eq}}\delta$ denote the barrier and equilibrium position for the thickness coordinate, respectively (see Fig. 6). This condition allows the calculation of a value of Φ'' such that spinodal dewetting takes place:

$$\Lambda = \sqrt{\frac{-8\pi^2\gamma}{n\Phi''(z_{\mathrm{b}})}}\,.$$

With our potential, for $\Delta\phi_{\mathrm{tot}} \approx k_{\mathrm{B}}T$, one gets $\Phi''(z_{\mathrm{b}}) = -2.6\cdot10^{10}$ J/m^2 so that $\Lambda \approx 12$ μm which is of the order of magnitude of the observed wavelength on the dewetting patterns (see, *e.g.*, Fig. 3).

4 Conclusion

We have shown that thin lipid films deposited on solid support are unstable in water-vapor atmosphere and can exhibit dewetting scenarios very similar to liquid crystalline and polymer films.

The present work comprises data of several sample series of the phospholipid DMPC. Dewetting was observed only in the fluid L_α phase, indicating that either the time scales are too long or that the stacks are stable in the low-temperature gel phase where fluctuations are reduced. Here we have shown that the observed dewetting can be explained by the effect of interfaces. In thin multilamellar

lipid systems the presence of interfaces implies a reduction of fluctuations and changes the equilibrium distance between the layers. As a consequence, it may affect the whole stability of the multilayer stack.

It should be noted that in principle, a similar discussion could be presented where the fluctuations are suppressed due to osmotic pressure, in line with interpretation b) of the vapor pressure paradox. The effect of osmotic pressure due to R.H. $\leq 100\%$, could be accounted for by adding a linear effective potential term ($V_{\text{eff}} = \Pi z$) in equation (8). A similar stability discussion as a function of vapor pressure could then be performed, with similar qualitative conclusions [42].

In this first-step study, we could not yet provide the experimental basis to fully clarify the dewetting mechanisms. In the next step, the eventual dewetting of charged bilayers and bilayers immersed in bulk water are obvious points to address. Furthermore, the time evolution should be quantified, *e.g.* by video-enhanced microscopy.

Finally, we note that the observations reported here, apart from the fundamental interest in understanding the thermal stability of model lipid membranes and to properly use them for structural studies, may have important implications for the technological use of solid-supported membranes. In this respect, a more precise control of the interaction potentials and the film stability is desirable.

References

1. M.J. Janiak, D.M. Small, G.G. Shipley, Biochem. J. **15**, 4575 (1976).
2. G. Fragneto, T. Charitat, F. Graner, K. Mecke, L. Perino-Gallice, E. Bellet-Amalric, Europhys. Lett. **53**, 100 (2001).
3. T. Hønger, K. Mortensen, J.H. Ipsen, J. Lemmich, R. Bauer, O.G. Mouritsen, Phys. Rev. E **72**, 3911 (1994).
4. F.Y. Chen, W.C. Hung, H.W. Huang, Phys. Rev. Lett. **79**, 4026 (1997).
5. R. Zhang, W. Sun, S. Tristram-Nagle, R.L. Headrick, R.M. Suter, J.F. Nagle, Phys. Rev. Lett. **74**, 2832 (1995).
6. R. Podgornik, V.A. Parsegian, Biophys. J. **72**, 942 (1997).
7. S. Tristram-Nagle, H.I. Petrache, R.M. Suter, J.F. Nagle, Biophys. J. **74**, 1421 (1998).
8. J.F. Nagle, J. Katsaras, Phys. Rev. E **59**, 7018 (1999).
9. A. Tardieu, V. Luzzati, F.C. Reman, J. Mol. Biol. **75**, 711 (1973).
10. G. Büldt, H.U. Gally, J. Seelig, G. Zaccai, J. Mol. Biol. **134**, 673 (1979).
11. G. Zaccai, G. Büldt, H.U. Gally, J. Seelig, J. Mol. Biol. **134**, 693 (1979).
12. J.F. Nagle, S. Tristram-Nagle, Biochim. Biophys. Acta **1469**, 159 (2000).
13. M. Vogel, C. Münster, W. Fenzl, T. Salditt, Phys. Rev. Lett. **84**, 390 (2000).
14. T. Salditt, C. Münster, J. Lu, M. Vogel, W. Fenzl, A. Souvorov, Phys. Rev. E **60**, 7285 (1999).
15. U. Mennicke, T. Salditt, submitted to Langmuir (2002).
16. K. He, S.J. Ludtke, D.L. Worcester, H.W. Huang, Biophys. J. **70**, 2659 (1996).
17. K. He, S.J. Ludtke, W.T. Heller, H.W. Huang, Biophys. J. **71**, 2669 (1996).
18. J. Penfold, R.K. Thomas, J. Phys. Condens. Matter **2**, 1369 (1990).
19. T. Charitat, E. Bellet-Amalric, G. Fragneto, F. Graner, Europhys. J. B **8**, 583 (1999).
20. E.B. Sirota, J. Chem. Phys. **105**, 7763 (1996).
21. F. Sommer, S. Alexandre, N. Dubreuil, D. Lair, Tran minh Duc, J.M. Valleton, Langmuir **13**, 791 (1997).
22. C. Braun, Parratt32 (1997-1999).
23. M. Born, E. Wolf, *Principles Optics* (Pergamon Press, Oxford, 1989).
24. V.F. Sears, Thermal-neutron scattering lengths and cross-sections for condensed-matter research, Chalk River Nuclear Laboratories, Chalk River, 1984.
25. J. Nagle, D.A. Wilkinson, Biophys. J. **23**, 159 (1978).
26. S. Herminghaus, K. Jacobs, K. Mecke, J. Bischof, A. Fery, M. Ibn-Elhaj, S. Schlagowski, Science **30**, 916 (1998).
27. F. Brochard-Wyart, J. Daillant, Can. J. Phys. **68**, 1084 (1989).
28. S. Dietrich, *Phase Transitions and Critical Phenomena*, Vol. **12** (Academic Press, London, 1988) pp. 1–218.
29. A. Vrij, Disc. Faraday Soc. **42**, 23 (1966).
30. F. Vandenbrouck, M.P. Valignat, A.M. Cazabat, Phys. Rev. Lett., **82**, 2693 (1999).
31. J. Israelachvili, *Intermolecular and Surface Forces*, second edition (Academic Press, London, 1992).
32. W. Helfrich, Natürforschung **33a**, 305 (1978).
33. M. Manciu, E. Ruckenstein, Langmuir **17**, 2455 (2001).
34. E.A. Evans, V.A. Parsegian, Proc. Natl. Acad. Sci. USA **83**, 7132 (1986).
35. T.J. McIntosh, A.D. Magid, S.A. Simon, Biophys. J. **55**, 897 (1989).
36. The theoretical ground of such functional dependence of the repulsive parts of the potential was shown to have some flaws [39]. A full systematic treatment of the interaction between two membranes including renormalized potential was developped by other authors [39,43].
37. H.I. Petrache, S. Tristam-Nagle, J.F. Nagle, Chem. Phys. Lipids **95**, 83 (1998).
38. J. Katsaras, Biophys. J. **75**, 2157 (1998).
39. R. Lipowsky, in *Handbook of Biological Physics*, Vol. **1b**, edited by R. Lipowsky, E. Sackmann (Elsevier Science, Amsterdam, 1995).
40. A. Poniewierski, R. Holyst, A.C. Price, L.B. Sorensen, S.D. Kevan, J. Toner, Phys. Rev. E **58**, 2027 (1998).
41. D.K.G. de Boer, Phys. Rev. E **59**, 1880 (1999).
42. This view is preferred by T. Salditt, arguing equation (11) is the dominant repulsive term in the system.
43. R.R. Netz, R. Lipowsky, Europhys. Lett. **29**, 345 (1995).